Eur Biophys J (1998) 27: 501–513

ARTICLE

Imre M. Jánosi · Denis Chrétien · Henrik Flyvbjerg

Modeling elastic properties of microtubule tips and walls

Received: 26 January 1998 / Accepted: 26 March 1998

Abstract Electron micrographs of tips of growing and shrinking microtubules are analyzed and interpreted. The many shapes observed are all consistent with a simple mechanical model, a flexible tube with competing intrinsic curvatures. Observations are also consistent with growing and shrinking microtubules having the same intrinsic curvature for protofilaments, the one observed in oligomers peeling off shrinking microtubules. If this is so, the lateral bonds between protofilaments are responsible for the difference between shapes of tips on growing and shrinking microtubules.

Key words Microtubule · Elasticity · Competing curvatures

I Introduction

Microtubules are the most rigid element of the cytoskeleton of eukaryotic cells. These tubular polymers give cells their shape, and provide stiffness to cilia and flagella. Dynein and kinesin motors haul vesicles along microtubules, exerting forces of ~1 piconewton, and during mitosis, the force that separates sister chromatids is also transmitted via microtubules. Since rigidity is what microtubules provide in most designs they are part of, much has been done to measure the rigidity of microtubules (Amos and Amos 1991; Dye et al. 1993; Gittes et al. 1993; Vale et al. 1994; Vernier et al. 1994; Kurachi et al. 1995; Bourdieu et al. 1995; Tran et al. 1995; Mickey and Howard 1995; Kurz and Williams 1995; Elbaum et al. 1996).

These works all treat microtubules in the *thin-beam approximation*, i.e., a microtubule is viewed as an infinitely thin, straight *fiber* and characterized by a single parameter, its flexural rigidity. This is not only a sensible approach, but the obly one possible, since the finer structure of microtubules cannot be resolved in the experiments done, nor can it be deduced from the data produced.

We know, however, since the discovery of microtubules with the electron microscope that they are small tubes. So a more refined description of microtubules would, as a natural next and finer level of approximation, describe them as small tubes with intrinsic mechanical properties that explain the observed and measured properties of microtubules.

Electron micrographs reveal much more than the tubular shape: they show that a microtubule is a two-dimensional, cylindrical "crystal" of proteins. But since electron micrography requires vitrified samples, observation in real time of micro-manipulations and their consequences, such as application of force to, e.g., the wall of a microtubule, is not possible.

Recent electron micrographs of *ends* of growing microtubules may, however, be interpreted to reveal mechanical properties of microtubules to a degree that goes beyond the thin-beam approximation. The micrographs show that growing ends of microtubules often taper to long, narrow tips that curve away from the microtubule; see Fig. 1 (Chrétien et al. 1995). These tips consist of protofilaments that are bound laterally to each other, but are too few in number to form a full microtubule. Their shapes reveal that conflicting elastic forces pull against each other within a microtubule's wall. More than this, the shapes are configurations in which the forces balance each other in this tug-of-war. So a quantitative analysis of many observed tip-

I. M. Jánosi · H. Flyvbjerg
Höchstleistungsrechenzentrum (HRLZ), Forschungszentrum Jülich, D-52425 Jülich, Germany

I. M. Jánosi (✉)
Department of Physics of Complex Systems, Eötvös University, Múzeum körút 6–8, H-1088 Budapest, Hungary

D. Chrétien
Cell Biology Program, European Molecular Biology Laboratory, D-69012 Heidelberg, Germany

H. Flyvbjerg
Condensed Matter Physics and Chemistry Department, Risø National Laboratory, DK-4000 Roskilde, Denmark

H. Flyvbjerg
The Niels Bohr Institute, Blegdamsvej 17, DK-2100 Copenhagen Ø, Denmark


200 nm

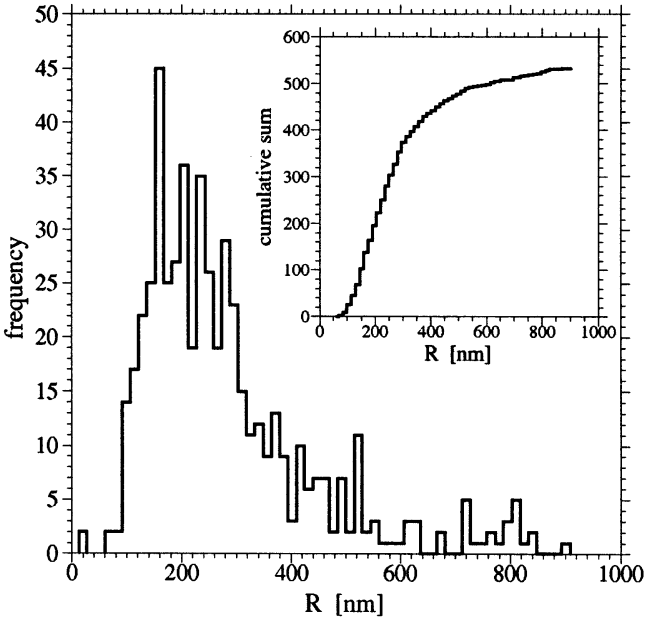

Fig. 2 Histogram of radii of curvature of microtubule tips read off electron micrographs. Radii are given in nanometers. The *inset* shows the cumulative sum for the same distribution

shares may reveal the elastic forces at play, despite the static nature of electron micrographs. Such an analysis is an attempt to deduce a cause from its consequences, hence a far from trivial exercise. We pursue it below, and obtain some definite qualitative results, and some ideas for further experiments prompted by these results and their derivation.

II Materials and methods

The images used in this work were taken from the study reported in Chrétien et al. (1995). It analyzed the mechanism of microtubule assembly by cryo-electron and video-light microscopy. Details concerning the preparation of the biological samples and the imaging conditions can be found in this article.

Good quality images at a final magnification of 66.000× were produced from the original negatives. Altogether 535 circularly bent microtubule extensions were identified. The radii of curvature were measured by comparing each extension with calibrated circles printed on a transparency and finding the circle providing the best fit. The accuracy of this simple measurement of radii was typically 1 mm, and limited by microtubule tip shapes being non-perfect sections of circles. The accuracy was better then 10% for every radius determined. Measurements were made for ten groups of microtubule tips, each group of tips being grown in a different tubulin concentration and/or for a different amount of time. Although different radii of curvature were found for different groups, the differences were not significant: The distribution of radii found for each group agreed with the aggregated distribution found by adding up all distributions from all groups. The latter distribution is shown in Fig. 2.

We have tried to determine the protofilament number of these uniformly curved microtubule extensions with a comparative contrast analysis. Owing to their large curvature, the sheets orient edge-on in the thin film of vitreous ice. Thus, the protofilament number could not be directly determined from the images. Attempts to interpret the contrast present in the images of the sheets in terms of protofilament numbers were also unsuccessful.

Fig. 1 View of the extremity of a microtubule aster grown for 1 min in a 19.5 μM tubulin solution. One notes the heterogeneity of the ends, which range from "blunt" to long, narrow, curved tips, formed by sheets of microtubule wall. One also notes that the longest of these curved tips are shaped as sections of circles

III Theory

In this section, we model the microtubule wall material as a two-dimensional elastic sheet with opposite intrinsic curvatures. Then we discretize this sheet model in order to treat it numerically, to find its minimum energy configuration. This we do first for sheet geometries that represent long microtubule tips with constant protofilament number, and eventually for a more generic microtubule tip.

Since the model contains several parameters, we need to know the solutions that we find depend on these parameters. In particular, we want to know if the qualitative results that we obtain are sensitive to our choice of parameter values. To this end, we study many tip shapes found numerically, and find that to a good approximation they have fairly simple geometries, as they are sections of tori. In the same approximation, the expressions for their elastic energies become fairly simple analytical expressions. From these analytical expressions we then prove mathematically that a wide range of parameter values result in the same qualitative behavior. Numerical results confirm this conclusion, and we are then ready to interpret observed microtubule tip shapes. That is the subject of the next section, and the reader only interested in results can skip the remainder of the present section.

A) The microtubule wall as an elastic sheet

We describe microtubules and tips with the same fundamental parameters. These characterize intrinsic elastic properties of the material from which microtubules and tips are formed. This material is an approximately 4 nm thick "sheet" of laterally connected protofilaments. We describe this material as a two-dimensional surface with mechanical properties that are the same everywhere (homogeneity), but differ with direction (anisotropy), because tubulin dimers and their bonds with each other are anisotropic.

From Fig. 1 and many similar micrographs one sees that many microtubule ends are sections of circles to a good approximation, and that these ends curve away from the axis of the microtubule. We interpret this as being due to *intrinsic curvature* of individual protofilaments. This curvature clearly does not favor the formation of the microtubule, as it tends to pull its constituent protofilaments away from each other.

On the other hand, microtubules do form spontaneously from tubulin in solution – i.e., with no template present. Protofilament numbers from 8 to 17 have been observed (Karecla et al. 1989; Chrétien and Wade 1991; Chrétien et al. 1992; Ray et al. 1993). The microtubules studied here were found to have from 10 to 16 protofilaments, with 13 or 14 protofilaments in 90% of the cases. The distribution of protofilament numbers had 13.45 as average, and 0.55 as RMSD. This spontaneous formation of tubes from solution we interpret in three respects : (i) Protofilaments must be elastic, since they can be straight with zero curvature in the wall of an integral microtubule, yet will curve out when permitted to do so in tips of growing and shrinking microtubules. (ii) The microtubule wall has an intrinsic *lateral* curvature that favors the formation of a cylinder. One can think of it as a property of the lateral bonds between protofilaments, but it may as well be due to a wedge-shaped cross section of protofilaments. This difference cannot be addressed and does not matter within the model used here. The existence of such an intrinsic lateral curvature is supported by electron micrographs of tubulin *sheets* that form when tubulin is allowed to polymerize from a relatively high initial concentration (Voter and Erickson 1984). These sheets are laterally curved with radius of curvature close to that of whole microtubules. (iii) The different protofilament numbers observed in spontaneously formed microtubules show that the microtubule wall material is flexible laterally: its actual curvature can differ from its intrinsic curvature, since microtubules with different protofilament numbers have different lateral radii of curvature, despite being made from the same material.

We model the microtubule wall-material with a two-dimensional elastic sheet with intrinsic longitudinal curvature c_{l0}, and intrinsic lateral curvature c_{t0}. These two intrinsic curvatures have opposite signs, giving the sheet negative *Gaussian* curvature, the mathematical expression for the kind of curvature that a horse saddle has – see Fig. 4 – as opposed to the positive Gaussian curvature of, e.g., surfaces of spheres and ellipsoids.

The preferred shape of this elastic sheet is the shape that minimizes its total energy E. This total energy is a sum of contributions for stretching and bending, $E = E_s + E_b$. The stretching energy can be written

$$E_s = \frac{1}{2}\int d^2 r\,(2\mu u_{ij}^2 + \lambda u_{kk}^2), \tag{1}$$

where μ and λ are the so-called two-dimensional Lamé coefficients, and u_{ij}, $i, j = 1, 2$, are the usual strain tensor elements derived from a displacement vector field $\mathbf{u}(\mathbf{r}) = (\mathbf{r}' - \mathbf{r})$ as $u_{ij} = 1/2\,(\partial_i u_j + \partial_i u_i + \partial_i u_k \partial_j u_k)$ (Landau and Lifshitz 1959). The bending energy is known as the Helfrich energy (Helfrich 1973)

$$E_b = \int d^2 r \left(\frac{1}{2}\kappa H^2 + \kappa_G K\right), \tag{2}$$

where κ and κ_G are the "usual" and the Gaussian (or saddle-splay) bending rigidities, respectively. H is the sum of the principal curvatures c_l and c_t, and $K = c_l c_t$ is the Gaussian curvature at a given surface point.

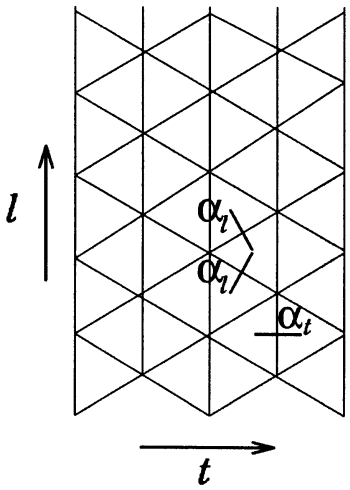

Fig. 3 Triangulation of a continuous surface with intrinsic curvature and anisotropic bending rigidities. l and t denote the longitudinal and transverse (lateral) directions, α_l and α_t denote the preferred (i.e., energy minimizing) angles between triangles sharing a longitudinally, respectively transversely, oriented edge. The other model parameters (not shown) are the bending stiffnesses of these angles, the preferred lengths of the triangles' edges, and the stiffness towards stretching or shortening of these edge lengths. Figure 4 shows a sheet formed such a triangulated surface in the configuration minimizing its total energy

We now wish to find the configuration of a given sheet that minimizes the sheet's elastic energy. Despite the simplifications introduced with this model, the model is too complex to allow us to solve this problem analytically. A numerical method must be employed. That done, we shall, however, see from the properties of the numerical solution that certain good approximations can be made, and within these approximation we can then do much analytically.

B) Lattice representation of elastic sheet

In order to describe the elastic sheet numerically, we discretized its surface with the triangulation shown in Fig. 3. We chose the edge-length of an unstretched triangle, i.e., the lattice spacing of the unstretched triangulation, as our unit of length, for a start. Intrinsic lateral curvature is built into the triangulation by introducing a preferred angle α_t between triangles that share an edge pointing in the longitudinal direction; see Fig. 3. This intrinsic lateral curvature gives rise to a corresponding preferred *radius* of lat-

eral curvature R_{t0}, which, in units of unstretched lattice spacings, is

$$R_{t0} = \frac{1}{c_{t0}} = \frac{\sqrt{3}}{4\sin(\alpha_{t0}/2)}. \quad (3)$$

Geometrical considerations also give a relationship between the radius of longitudinal curvature, R_{l0}, and the preferred angle α_l between triangles that share an edge pointing in a transverse direction; see Fig. 3:

$$\cos^2\frac{\alpha_{l0}}{2} = \frac{4}{3}R_{l0}^2(\sin^2 3\beta - \sin^4\beta) + \frac{1}{4}, \quad (4)$$

where $2\sin 2\beta = R_{l0}^{-1}$. α_{l0} and α_{t0} have opposite signs, like c_{l0} and c_{t0}.

The elastic *bending energy* of the continuous sheet is modeled with the two-dimensional triangular lattice by associating an energy with each angle between triangles that share an edge. The exact form of this energy does not matter, as long as it is quadratic in the displacement near its minimum, because we shall consider only small displacements, which then experience a restoring force obeying Hooke's Law. It is convenient to express this bending energy in terms of the unit normals to each elementary triangle. A simple choice is

$$E_b^{\text{lattice}} = \frac{1}{2}\kappa' \sum_{(\alpha,\beta)} \left|\mathbf{n}_\alpha - \mathbf{n}_\beta\right|^2, \quad (5)$$

where the sum is over all pairs of triangles sharing an edge, and κ' is the lattice bending rigidity.

Seung and Nelson (1988) proved that for an isotropic two-dimensional triangular lattice $\kappa_G = -\kappa$, i.e., the continuum limit of Eq. (5) is

$$E_b = \frac{1}{2}\kappa\int d^2 r\,(H^2 - 2K), \quad (6)$$

with

$$\kappa = \frac{\sqrt{3}}{2}\kappa'; \quad (7)$$

compare Eq. (2).

As a consequence, the total bending energy E_b can be decomposed in two partial energies and expressed in terms of the principal curvatures in an appropriately chosen curvilinear coordinate system,

$$E_b = E_{bl} + E_{bt} = \frac{1}{2}\kappa\int d^2 r c_l^2 + \frac{1}{2}\kappa\int d^2 r c_t^2. \quad (8)$$

In the case of nonzero intrinsic curvatures c_{l0} and c_{t0}, the last equation is replaced by

$$E_b = \frac{1}{2}\kappa\int d^2 r\,(c_l - c_{l0})^2 + \frac{1}{2}\kappa\int d^2 r\,(c_t - c_{t0})^2. \quad (9)$$

The elastic *stretching energy* of the sheet is modeled by

$$E_s^{\text{lattice}} = \frac{1}{2}\varepsilon \sum_{(a,b)} \left(|\mathbf{r}_a - \mathbf{r}_b| - 1\right)^2, \quad (10)$$

where the sum is over all bonds (a, b) between nearest neighbour vertices a and b of the lattice, and ε is the microscopic stretching rigidity. Consequently, any stretching or compression of any bond in the lattice will result in a restoring force obeying Hooke's Law with coefficient ε. Equation (10) has Eq. (1) as continuum limit with (Seung and Nelson 1988)

$$\mu = \lambda = \frac{\sqrt{3}}{4}\varepsilon. \quad (11)$$

This identity between the Lamé coefficients is due to our choice of identical stretching rigidity ε for all lattice bonds, irrespective of their orientation. This identity in only indirectly based on empirical insight, and is rather due to a wish not to introduce unnecessary parameters. The microtubule wall is certainly not isotropic. On the contrary, we expect its stretching stiffness in the longitudinal direction to differ from its stretching stiffness in the transverse direction. However, the lattice stiffness must be rather high for the model microtubule to largely retain the shape of its cross section when bending moderately, as real microtubules do. Preempting results, we consequently find that transversely oriented bonds essentially do not change their lengths in our simulations. But that behavior would result from *any* large value for the transverse stretching stiffness, i.e., its value does not matter, does not affect the configurations we find, as long as its value is large. Being about as large as the longitudinal stretching stiffness is sufficient, we found, so we used the latter's value also for the transverse stiffness. This result carries into a qualitative result about real microtubules: we except the tubulin dimers and the bonds between protofilaments to be about as stiff or stiffer towards transverse stretching as the protofilaments themselves are towards longitudinal stretching.

Now, given values for the intrinsic curvatures α_l and α_t, and for the stiffnesses towards stretching and bending, ε and κ', the preferred shape of a sheet is found by minimizing the triangulated sheet's total elastic energy

$$E = E_s^{\text{lattice}} + E_{bl}^{\text{lattice}} + E_{bt}^{\text{lattice}}. \quad (12)$$

The stretching energy E_s^{lattice} is the one given in Eq. (10). The bending energies are of the form given in Eq. (5), except we introduce intrinsic curvature by giving the bending energies minima for non-zero bending angles,

$$E_{bl}^{\text{lattice}} = \frac{1}{2}\kappa' \sum_{(\alpha\neq\beta)} \left(\left|\mathbf{n}_\alpha \times \mathbf{n}_\beta\right| - \sin\alpha_{l0}\right)^2, \quad (13)$$

for bending at longitudinally oriented edges/bonds, and an identical expression for transversely oriented bonds, with subscript 1 replaced by t.

C) Energy minimization, numerical method

The configuration of a given sheet that minimizes its total elastic energy was found with a conjugate-gradient relaxation method (Press et al. 1992) that involves all variables

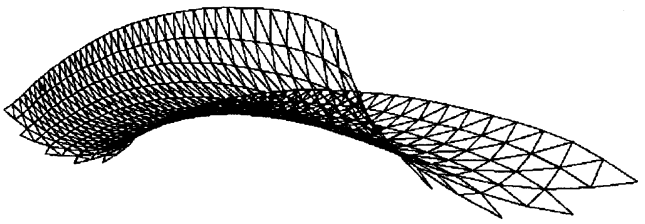

Fig. 4 Minimum energy configuration of a triangulated elastic sheet having $L_0 = 40$, $W_0 = 5\sqrt{3}$, $\kappa'/\varepsilon = 0.07$, $\alpha_t = 2\pi/28$ (i.e., $R_{t0} = 3.87$), and $\alpha_l = 0.1$ (i.e., $R_{l0} = 3.867$).(Lengths are here given in units of an unstretched lattice bond.)

$\mathbf{r}_a$ in each relaxation step, i.e., configuration updates are *global*. We found this algorithm to be the most efficient one compared to simpler, local algorithms. The reason for this efficiency is easily understood in physical terms: low-energy deformations of the energy-minimizing configuration are coherent, "long wave length" deformations, i.e., global deformations. Elimination of such deformations is the bottleneck in the process of finding the minimum-energy configuration with any local algorithm, and is only done efficiently with an algorithm that can find and move in the few degrees of freedom characterizing "long wavelength" deformations, i.e., a global algorithm.

Figure 4 shows a typical minimum-energy configuration for a small, rectangular-shaped sheet. Note that bond-lengths and -angles typically *differ* from their preferred values even in a configuration of the sheet that minimizes its energy. This is because the opposite intrinsic curvatures give rise to a tug-of-war within the elastic sheet, i.e., in the material of the microtubule's wall, and this tug-of-war results in a compromise with no side winning it all. Thus, a microtubule that is left undisturbed by external forces is nevertheless under tension from its internal forces!

We studied long, rectangular sheets as models for long microtubule tips with constant protofilament number along their lengths. These sheets differed from the small one shown in Fig. 4 only through their values for L_0 and W_0, and for some of them also through the values for their intrinsic curvatures and stiffnesses. But we mostly chose the intrinsic curvatures such that $R_{t0} = 1.6\, R_{l0}$, because electron micrographs show that the radius of curvature of isolated protofilaments protruding from ends of depolymerizing microtubules is approximately 0.8 times the microtubule diameter.

Thus we here investigate the hypothesis that the intrinsic curvature of protofilaments in growing and shrinking microtubules is the same, and equal to the large curvature observed in oligomers falling off shrinking microtubules. We find that this hypothesis and its consequences for microtubule tip shapes is not contradicted by observed microtubule tip shapes.

D) Analysis of energy-minimizing lattice configurations

In order to characterize the geometry of a rectangular sheet's energy-minimizing configuration, we evaluated its local curvatures. We did this for several sheets. Figure 5 shows typical results for a small sheet, local values for the principal radii of curvature, R_l and R_t, at various positions along and across the sheet shown in Fig. 4. Towards the edges and ends of the sheet, these actual curvatures approach the sheet's intrinsic curvatures. Away from edges and ends, on the other hand, the actual curvatures are approximately constant, as one would expect from a homogeneous sheet with constant width. We note that $R_t/R_{t0} \approx 1$ while $R_l/R_{l0} \gg 1$ for the parameter values we have chosen for the intrinsic curvatures and the bending and stretching rigidities. These values were chosen in a range where the resulting tip shapes qualitatively resemble those of observed microtubule tips. Below, we show analytically that a range of parameter values result in the same qualitative behavior, so our results are not that sensitive to the specific values chosen for parameters, as long as they are chosen in certain ranges.

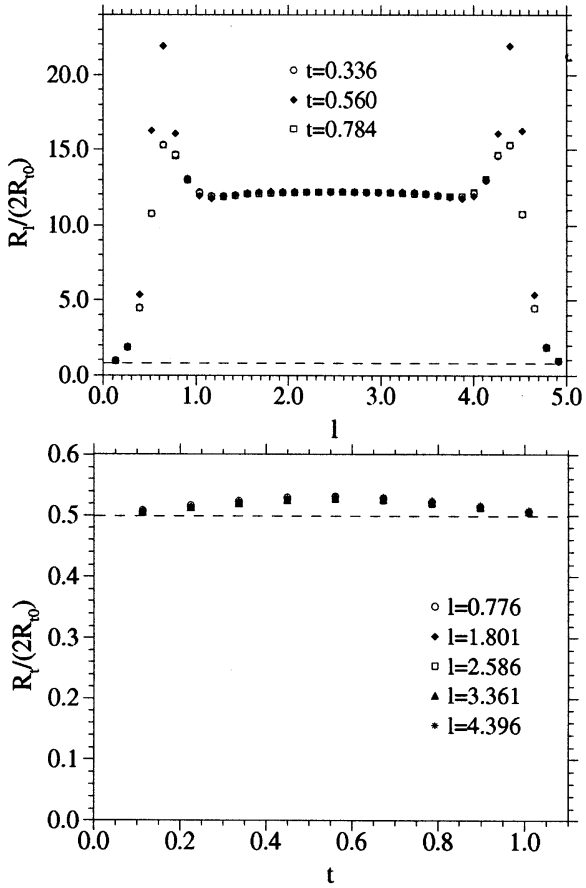

Fig. 5 *Top*: Local longitudinal radius of curvature R_l, as a function of longitudinal coordinate *l* along the sheet shown in Fig. 4, given at three different lateral coordinates *t*. The *dashed lines* indicate the radius of intrinsic curvature, $R_{l0} = 0.80$. Lengths and coordinates in this plot are given in units of $2R_{t0}$, a microtubule diameter. *Bottom*: Local lateral radius of curvatures R_t, as a function of lateral coordinate *t* across the sheet, given at five different longitudinal coordinates *l* along the sheet shown in Fig. 4. The *dashed line* indicates the radius of intrinsic curvature, $R_{t0} = 1/2$, in units of $2R_{t0}$

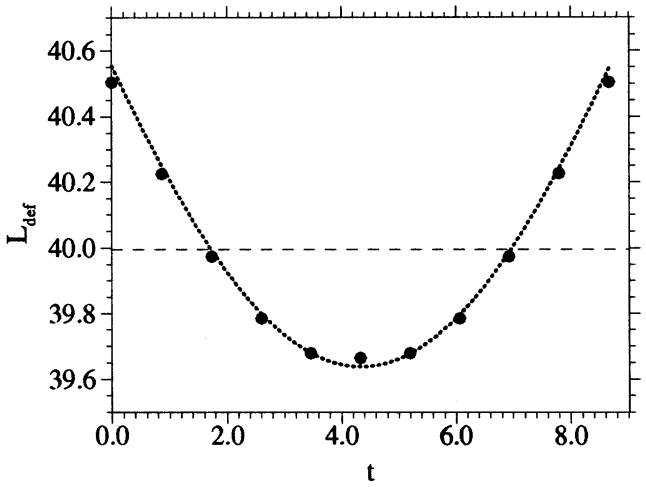

Fig. 6 Filled circles: Total length L_{def} of the 40 longitudinal bonds at a given lateral coordinate t in the triangulated sheet shown in Fig. 4. The unit of length used here is one unstretched lattice bond. *Horizontal dashed line:* The unstretched and uncompressed length L_0 = 40. *Dotted line:* Eq. (14) with $\theta_0 = 0.205$, $R_m = R_l + R_t = 100.63$ and $R_t = 3.945$

As for stretching and compression of bonds, we found effectively none of that for transverse bonds, only relative deformations of order 10^{-4} and less, growing to about 0.5% at the very ends of the sheet. The very ends of the sheet are of no interest to us for now, so these deformations are negligible compared to the deformations of longitudinal bonds, which are of order 1%; see Fig. 6. Figure 6 shows how the sheet shown in Fig. 4 is stretched or compressed longitudinally as a function of the lateral coordinate whithin the sheet. As it to be expected for the configuration in Fig. 4, longitudinal bonds near the edge of the sheet are stretched, while those near its center are compressed. The corresponding forces of opposite sign balance each other, i.e., sum to zero, because no external forces act on the sheet. Since forces obey Hooke's Law, i.e., are proportional to deformations, the deformations shown in Fig. 6 sum to zero. This zero sum, together with the unchanged width of the sheet, explains why we found the *area A* of the sheet virtually unchanged by the stretching and compression of bonds: $(A - L_0 W_0)/(L_0 W_0) \approx 10^{-4} - 10^{-5}$. The dotted line in Fig. 6 is explained below.

We found and analyzed the minimum-energy configuration of several sheets of different sizes and with different elastic parameters in the manner just described. We also studied different discretizations of a given sheet, and all our observations suggest that the minimum-energy configurations to a good approximation can be characterized geometrically in a manner that is much simpler than the manner it was found, namely, as a section of a torus, as we just demonstrated for the sheet in Fig. 4. Assuming a section-of-torus geometry, we have a simple analytical description of the energy-minimizing configuration. Having that, we can *repeat* the search for this configuration with *analytical* methods. We restrict the search to section-of-torus geometries, and we use the fact that these simple geometries have correspondingly simple analytical expressions for their elastic energies.

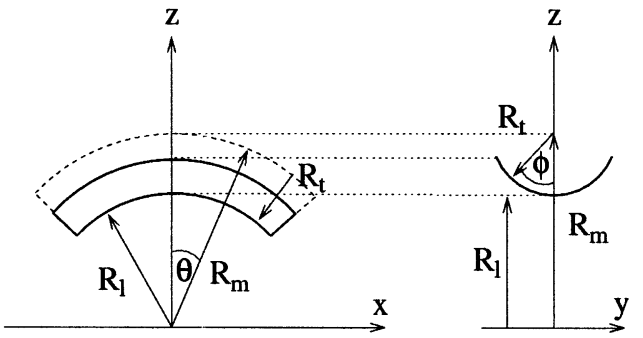

Fig. 7 One possible parametrization of a section of a torus; see text for details

E) Simplifying analytical approximation

Figure 7 shows one possible parametrization of a section of a rotation-symmetric torus with circular cross-section. Each point on the torus' surface can be parametrized by two angles, $\phi \in [-\phi_0, \phi_0]$ and $\theta \in [-\theta_0, \theta_0]$. In the Euclidean coordinate system shown in Fig. 7, the same point's coordinates, (x, y, z), are given by its angles as $x = (R_m - R_t \cos\phi) \sin\theta$, $y = -R_t \sin\phi$, and $z = (R_m - R_t \cos\phi) \cos\theta$. Here R_m denotes the "main" radius of curvature of the center of the torus, and R_t is the radius of the cross section. Note that R_l, the principal radius of curvature in the longitudinal direction, is different from the "main" radius $R_m = R_l + R_t$.

For a generic section of a torus, the parameters (θ, ϕ) are, of course, not restricted to a rectangle $[-\theta_0, \theta_0] \times [-\phi_0, \phi_0]$, as they are for the section shown in Fig. 7. But they are for the rectangular sheets that we studied. This is not altogether obvious, but is demonstrated by the dotted line in Fig. 6 for the sheet in Fig. 4, and follows also from theoretical considerations: The only way that a long, homogeneous sheet can be stretched, compressed, and bent into the shape shown in Fig. 4 with local deformations that are the same all along its length, and independent of its length, is if its ends are shaped as if cut by a plane through the axis of rotation of the torus, as in Fig. 7. This geometry translates into a mathematical statement,

$$L_{def}(\phi) = 2\theta_0 (R_m - R_t \cos\phi), \tag{14}$$

where $L_{def}(\phi)$ is the total length of the torus section along a line with constant ϕ-value.

The dotted line in Fig. 6 is the graph of $L_{def}(\phi)$ in Eq. (14) with R_t and $R_m = R_l + R_t$ read off Fig. 5, and $\theta_0 = 0.205$, with $\langle L_{def} \rangle$ the average over ϕ of the values for $L_{def}(\phi)$ shown in Fig. 6.

The elastic energies of a sheet shaped as a section of a torus have fairly simple analytical expressions, especially when we ignore lateral stretching, as we will, because we

found it negligible for the elastic parameter values of interest here.

The stretching energy then involves only longitudinal stretching:

$$E_s(R_m, R_t, \theta_0) = \frac{\mu}{2} L_0 R_t \int_{-\phi_0}^{\phi_0} d\phi \left[\frac{2\theta (R_m - R_t \cos\phi)}{L_0} - 1 \right]^2, \tag{15}$$

where ϕ_0 reflects to unchanged width of the sheet,

$$2\phi_0 = \frac{W_0}{R_t}. \tag{16}$$

The bending energies E_{bl} and E_{bt} in Eq. (9) are now simple functions of the principal radii of curvature. With

$$c_t = \frac{1}{R_t} \tag{17}$$

and

$$c_l(\phi) = \frac{-\cos\phi}{R_m - R_t \cos\phi}, \tag{18}$$

the transverse bending term is especially simple:

$$E_{bt} = \frac{\kappa}{2} L_0 W_0 \left(-\frac{1}{R_t} - \frac{1}{R_{t0}} \right)^2. \tag{19}$$

(We have chosen c_{t0} positive and c_{l0} negative; only their relative signs matter.) The longitudinal bending energy is

$$E_{bl} = \frac{\kappa}{2} L_0 R_t \int_{-\phi_0}^{\phi_0} d\phi \left(\frac{\cos\phi}{R_m - R_t \cos\phi} - \frac{1}{R_{l0}} \right)^2. \tag{20}$$

An energy-minimizing configuration of the section-of-torus sheet is given by the values for R_l, R_t, and θ_0 that minimize the total elastic energy, the sum of E_s, E_{bt}, and E_{bl}. Since θ_0 appears only in E_s, it can be determined as a function of R_l and R_t from the extremum condition

$$\frac{\partial E_s}{\partial \theta_0} = 0 \tag{21}$$

and eliminated from the minimization problem. That done, the minimizing values for R_l and R_t were found numerically.

F) Dimensional analysis

Before we used numerical methods to find energy-minimizing configurations, of triangulated sheets or sections of tori, we considered the exact analytical simplifications of the problem provided by dimensional analysis. We are considering a system that has dimensions *length* and *energy* associated with it, and several dimensionfull parameters occur in its definition: the intrinsic radii of curvature, the bond length in the case of the lattice, the stiffnesses κ and μ, or ε. The dimension of κ is *energy*, while that of μ is (*energy*)/(*length*)^2. Consequently, we can choose to measure all energies in units of κ and all lengths in units of $2R_{t0}$. That leaves us with only one, dimensionless stiffness parameter to vary,

$$\tilde{\mu} = \mu (2R_{t0})^2 / \kappa, \tag{22}$$

and two dimensionless intrinsic length scales, $\tilde{R}_{l0} = R_{l0}/(2R_{t0})$, which we mostly chose to fix at the value 0.8 for reasons given above, and the width of the sheet, $\tilde{W}_0 = W_0/(2R_{t0})$. Since the sheet is homogeneous, i.e., has the same intrinsic properties everywhere, results for its radii of curvature do not depend on its length L_0.

The energy-minimizing values for $\tilde{R}_l = R_l(2R_{t0})$ and $\tilde{R}_t = R_t/(2R_{t0})$ do not depend on the overall value of the total energy, since a minimum remains a minimum when a function is multiplied by a positive factor. Consequently, $\tilde{R}_l$ and $\tilde{R}_t$ do not depend directly on κ, but only on $\tilde{\mu}$ and on $\tilde{W}_0$, i.e., on a total of two parameters, three if we choose to vary $\tilde{R}_{l0}$ as well.

Our choice of $2R_{t0}$ as unit of length was motivated by the relative ease with which it can be obtained in electron micrographs as the microtubule diameter.

G) Solutions

Figure 8 gives the energy-minimizing values for $\tilde{R}_l$ and $\tilde{R}_t$ as functions of the sheet's width $\tilde{W}_0$ for various values of $\tilde{\mu}$. Values obtained by energy minimization of the triangulated sheet model are shown as plotting symbols. Values obtained in the section-of-tours approximation are shown as full lines. The two kinds of results agree more than sufficiently for our mainly qualitative purposes, especially for $\tilde{R}_l$, which is fortunate, since it is the radius of curvature that is most easily observed experimentally. Discrepancies between the two descriptions occur at relatively narrow widths, where discretization errors introduced with the triangulation of the continuous sheet are relatively important. These errors can be reduced by employing a finer triangulation, but that is fairly pointless, since the real microtubule wall is not homogeneous laterally, but is made from protofilaments, and we consequently expect experimental results for narrow tips to differ as well from our description in terms of a continuous sheet.

The dashed lines in Fig. 8 show the power law dependencies $R_l/R_{l0} \propto \tilde{W}_0^4$ and $\tilde{R}_t - \tilde{R}_{t0} \propto \tilde{W}_0^{-4}$, which we return to below. For reasons also given below, we found it convenient to plot the particular combinations of radii shown in Fig. 8, instead of just $\tilde{R}_l$ and $\tilde{R}_t$.

Figure 9 shows the same quantities as Fig. 8 does, but for four different values of $\tilde{R}_{l0}$, while $\tilde{R}_{l0}$ was fixed at the value 0.8 in Fig. 8. Only results for two different values of $\tilde{\mu}$ are shown, but the conclusions should be clear from the figure: there is an almost perfect scaling collapse between results obtained for different values of $\tilde{R}_{l0}$, and qualitatively the very same behavior for different values of $\tilde{\mu}$ – in the range probed here, at least. These are very positive results, because they illustrate that even beyond the results of the dimensional analysis, the results obtained with our

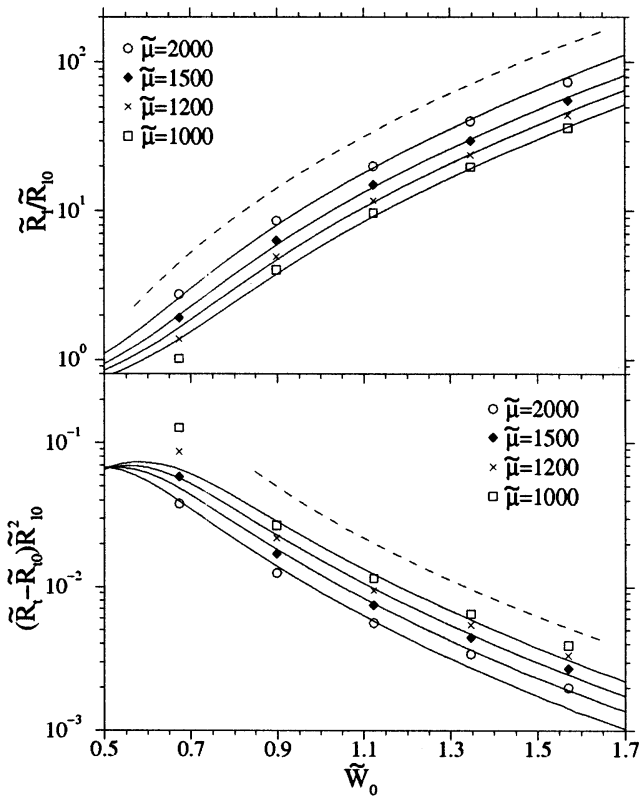

Fig. 8 Comparison of full treatment of elastic sheet, discretized as triangular lattice (results shown with *plotting symbols*), and continuous treatment of elastic sheet, approximated as a section of a torus (results shown as *continuous lines*). As functions of sheet width $\tilde{W}0$, we show: *Top frame:* The radius of longitudinal curvature $\tilde{R}_l$ for the energy-minimizing configuration, in units of the radius of intrinsic longitudinal curvature $\tilde{R}_{l0}$. *Bottom frame:* The difference between the radius of transverse curvature, $\tilde{R}_t$, of the energy-minimizing configuration, and the radius of intrinsic curvature, $\tilde{R}_{t0} = 1/2$, multiplied by a factor $\tilde{R}^2_{l0}$ for reasons given in the text. Lengths are measured in units of $2R_{t0}$, as indicated with the tildes. The *dashed lines* show simple power-laws, $\propto \tilde{W}_0^4$ (*top*), and $\propto \tilde{W}_0^{-4}$ (*bottom*)

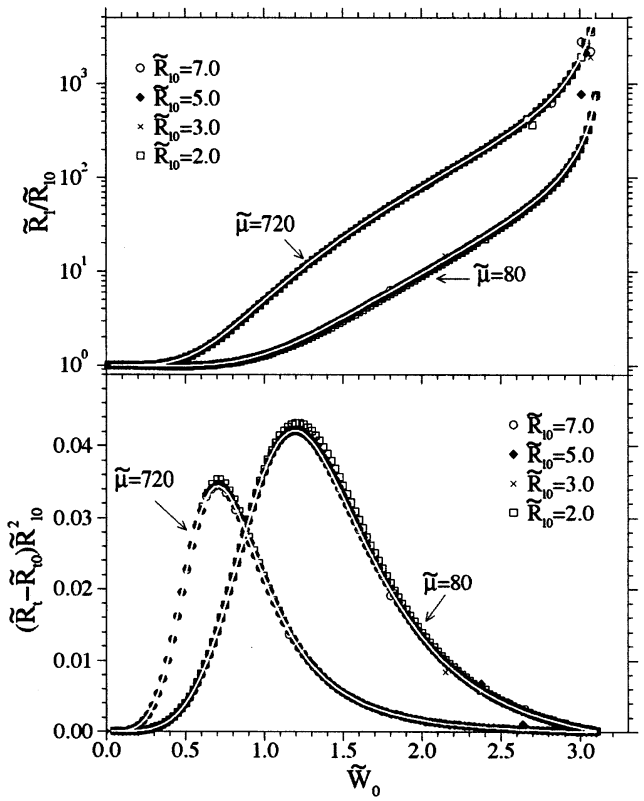

Fig. 9 Dependence of the radii $\tilde{R}_l$ and $\tilde{R}_t$, on the width $\tilde{W}_0$ for energy-minimizing configurations of rectangular elastic sheets. Results are shown for two different values of the dimensionless stiffness $\tilde{\mu}$, and for four different values for the dimensionless radius $\tilde{R}_{l0}$ of intrinsic longitudinal curvature. Note the collapse of data for different values of $\tilde{R}_{l0}$. The curves drawn in white through the data points are given by Eqs. (25) and (26). All lengths are given in units of $2R_{t0}$, so when $\tilde{W}_0$ approaches π, a whole, hence straight, tube can form, and does indeed, as we see from $\tilde{R}_l \to \infty$ and $\tilde{R}_t \to \tilde{R}_{t0}$

model are general, do not depend on particular choices for parameter values.

Before we discuss what those results are, according to Fig. 9, we explain the origin of its scaling collapses, and derive approximate analytical expressions for the results shown.

H) Further analytical simplifications

In the present analysis, we have always chosen values for $\tilde{\mu}$ and $\tilde{R}_{l0}$ such that the resulting tubes and sheets have the same qualitative properties as microtubules and microtubule tips. For example, the stiffnesses towards deformations should favor that a long, rectangular sheet that is wide enough to form a significant part of tube, indeed does that, as illustrated in Fig. 10. With a different choice of values for these parameters, such a sheet may flatten transversely and roll up longitudinally as a long "serpentine", effectively a tube of length W_0 and diameter $2R_{l0}$.

Figure 9 shows that for narrow widths W_0, the radius of longitudinal curvature, R_l, is essentially constant, independent of W_0, and equal to is intrinsic value R_{l0}. So a long and sufficiently narrow strip will, indeed, roll up as a long "serpentine". But for somewhat wider strips, R_l increases exponentially fast with increasing $\tilde{W}_0$. In the case of $\tilde{\mu} = 180$, we see that the transition from constant to exponentially increasing $\tilde{R}_l$ occurs at $\tilde{W}_0 \approx 0.5 \approx 2\pi/13$, i.e., a strip the width of one protofilament will roll up with curvature very close to its intrinsic one, while already a strip with the width of two protofilaments will roll up with a several times larger radius of curvature.

Now consider the term

$$R_m - R_t \cos\phi = R_l + R_t(1 - \cos\phi)$$

that occurs in the expressions for E_s and E_{bl} in Eqs. (15) and (20) above. Since

$$|\phi| \le \phi_0 = W_0/(2R_t) \le W_0/(2R_{t0}) = \tilde{W}_0, \qquad (23)$$

small widths $\tilde{W}_0$ ensure that $R_l \gg R_t(1 - \cos\phi)$ because $1 - \cos\phi \le \phi^2/2 \le \phi_0^2/2 \le \tilde{W}_0^2/2 \ll 1$, while $R_l \ge R_{l0} \ge R_{t0} \approx R_t$. Widths that are *not* small, on the other hand, have

$R_l \gg R_{l0} \geq R_{t0} \approx R_t$, while $0 \leq 1 - \cos\phi \leq 2$, so also in this case in $R_t \gg R_t(1 - \cos\phi)$. Together, the two cases exhaust all possibilities, and we consequently use the approximation

$$R_l + R_t(1 - \cos\phi) \approx R_l \tag{24}$$

in the stationarity conditions $\partial E/\partial R_l = \partial E/\partial R_t = \partial E/\partial \theta_0 = 0$ that define the energy minimizing values for R_l, R_t, and θ_0. Here $E = E_s + E_{bl} + E_{bt}$, and it is important that the approximation (24) is done *not* in the energy E itself *before* it is differentiated to obtain the stationarity conditions, but only in these conditions *after* they have been derived. This is because a small quantity like $R_l + R_t(1 - \cos\phi)$ can have a significant derivative. For example is its derivative with respect to R_l is equal to 1.

Within the approximation just described we then find, after some algebra, that

$$R_l/R_{l0} = I_2/I_1 + \tilde{\mu}\,(I_2 - I_1^2)/(4I_1) \tag{25}$$

and

$$(\tilde{R}_t - \tilde{R}_{t0}) - \tilde{R}_{l0}^2 = \frac{1}{16}\left(\frac{2(I_1 - \cos\tilde{W}_0)}{\tilde{R}_l/\tilde{R}_{l0}} - \frac{I_2 - \cos^2\tilde{W}_0}{(\tilde{R}_l/\tilde{R}_{l0})^2}\right) + \frac{\tilde{\mu}}{64}\frac{(I_1 - \cos\tilde{W}_0)^2 - 3(I_2 - I_1^2)}{(\tilde{R}_l/\tilde{R}_{l0})^2} \tag{26}$$

where we have introduced the notation I_n, $n = 1, 2$, for the integrals

$$I_n = \int_0^{\tilde{W}_0} \frac{d\phi}{\tilde{W}_0}\cos^n\phi = \begin{cases} \dfrac{\sin\tilde{W}_0}{\tilde{W}_0} & \text{for } n = 1 \\ \dfrac{1}{2}\left(1 + \dfrac{\sin(2\tilde{W}_0)}{2\tilde{W}_0}\right) & \text{for } n = 2 \end{cases} \tag{27}$$

Thus we finally have an analytical description in closed form of the not-so-trivial dependence of the principal curvatures on the sheet's width and on the model's single dimensionless parameter, $\tilde{\mu}$. We note that according to this description, $\tilde{R}_l/\tilde{R}_{l0}$ diverges at $\tilde{W}_0 = \pi$ because I_1 in the denominator in Eq. (25) vanishes for $\tilde{W}_0 = \pi$. This divergences is also seen numerically in Fig. 9, and signals that a straight microtubule is formed when the sheet is wide enough to form one, i.e., for $W_0 = 2\pi R_{t0}$, or, equivalently, $\tilde{W}_0 = \pi$.

Using these analytical results, we should now be able to explain the approximate power law dependencies observed in Fig. 8. These approximate power laws are good approximations only for $\tilde{W}_0 > 0.7$ or so. But that bound is also about the smallest width at which we can expect our continuous sheet to approximate laterally bound protofilaments reasonably well, since it is the width of three protofilaments. So the simplification represented by these power laws may be useful, and we consequently seek out their origin.

It is fairly simple, and is partly revealed by the $\tilde{\mu}$-dependence of the curves in Fig. 8. We note that curves corresponding to different values of $\tilde{\mu}$ are separated by a vertical spacing that is approximately independent of $\tilde{W}_0$ for $\tilde{W}_0 > 0.7$. This means that the $\tilde{\mu}$-dependence of the plotted quantities is through a simple factor that does not depend on $\tilde{W}_0$. Moreover, we observe that $\tilde{R}_l/\tilde{R}_{l0}$ is approximately proportional to $\tilde{\mu}$, while $(\tilde{R}_t - \tilde{R}_{t0})\tilde{R}_{l0}^2$ is approximately proportional to $\tilde{\mu}^{-1}$. So it is clear what to look for in Eqs. (25) and (26). For $\tilde{\mu}$ as large as in Fig. 8, the second term on the right-hand-side of Eq. (25) is much larger than the first term when $\tilde{W}_0$ is not too small, hence makes $\tilde{R}_l/\tilde{R}_{l0}$ proportional to $\tilde{\mu}$, as observed numerically. In Fig. 8, $\tilde{W}_0$ is not large, so an expansion in $\tilde{W}_0$ to leading order may be a decent approximation. It yields

$$R_l / R_{l0} \approx \frac{\tilde{\mu}}{180}\tilde{W}_0^4, \tag{28}$$

i.e., the sought-for power law.

With R_l/R_{l0} thus proportional to $\tilde{\mu}$, the first and last terms in Eq. (26) are proportional to $\tilde{\mu}^{-1}$, while the second term is ignorable compared to them. Thus $(\tilde{R}_t - \tilde{R}_{t0})\tilde{R}_{l0}^2$ is proportional to $\tilde{\mu}^{-1}$, as expected. Expanding in $\tilde{W}_0$ to leading order, we find that only the last term in Eq. (26) contributes, yielding

$$(\tilde{R}_t - \tilde{R}_{t0})\,\tilde{R}_{l0}^2 = \frac{45}{2\tilde{\mu}\,\tilde{W}_0^4}, \tag{29}$$

i.e., the other sought-for power law.

Tracing back the origin of the contributing terms in these results, we see that the simple proportionality with $\tilde{W}_0^4$ and $\tilde{\mu}$ observed in the top frame in Fig. 8, and with $\tilde{W}_0^{-4}$ and $\tilde{\mu}^{-1}$ in the bottom frame, is due to dominance of the stretching energy over the longitudinal bending energy. Thus we conclude that if protofilaments willingly bend, but are unwilling to stretch and unwilling to change the intrinsic lateral curvature of the sheets they form, then we should expect a simple fourth power dependence of the radius of curvature of tips with their widths. Conversely, if such a dependence were observed, we would know how to interpret it, and could presumably also rule out other explanations. Unfortunately, things are not that simple. But now we are prepared in discuss them.

IV Results

A) Thermal fluctuations ignored

Figure 10 illustrates in a three-dimensional manner the very strong dependence of a microtubule tip's longitudinal radius of curvature R_l on the tip's width W_0, as found in the previous section. We emphasize that all of the model tips shown in Fig. 10 have the same "material" properties, namely the same stiffnesses and the same intrinsic radii of curvature. The circularly bent sheet representing a single protofilament has a $\tilde{R}_l = \tilde{R}_{l0} = 0.8$ microtubule diameters.

Now that we have understood the behavior of model tips of constant width, we are prepared to study more com-

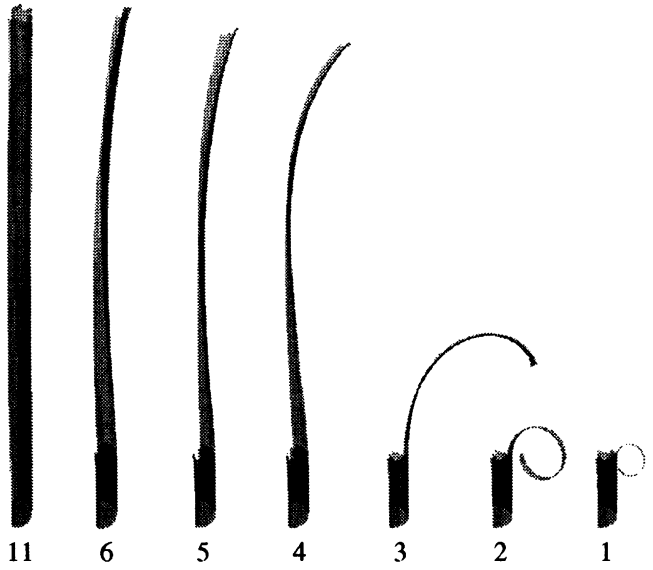

Fig. 10 Minimum energy configurations of model microtubule tips of different uniform widths: 1, 2, 3, 4, 5, 6, and 11 protofilaments. All tips shown have the same intrinsic properties. (The length scale is given by the diameter of the short piece of closed tube each tip is attached to.) Different tip widths result in different longitudinal curvatures, despite all tips having the same *intrinsic* longitudinal curvature. (All tips have been given a slight twist for better 3d perspective, and do not have constant R_l along their lengths, because they are attached to closed tubes at one end, and sensitive to this boundary condition.)

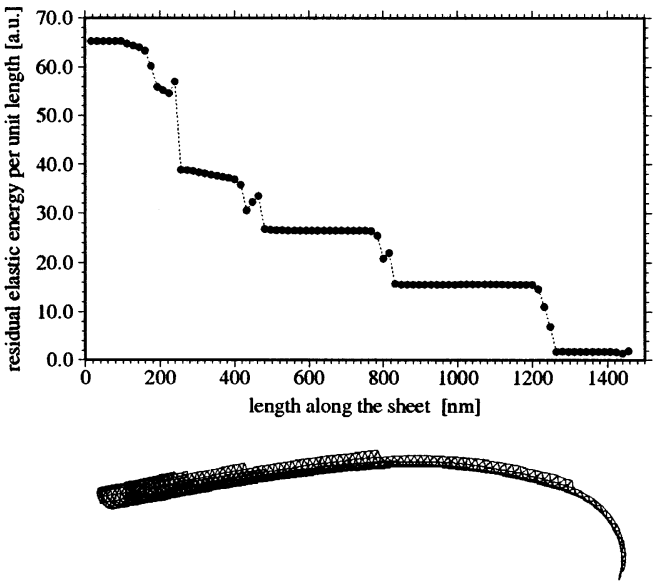

Fig. 11 The minimum energy configuration for a model microtubule tip of gradually decreasing width, and its local residual elastic energy (in arbitrary units). The intrinsic elastic properties and intrinsic curvatures are the same everywhere in this model tip, but the actual, realized curvatures are not, because they depend on the tip's width and its shape in general. Consequently, the amount of local residual elastic energy of the configuration also varies along its length, decreasing towards the end. (The length scale is given by the diameter of the short piece of closed tube on the left end.)

plicated tip configurations. Such configurations can only be studied numerically, using the triangulated sheet model. As one example, we show in Fig. 11 the energy-minimizing configuration of a model tip with a gradually decreasing protofilament number. The local residual elastic energy of the configuration is also shown as a function of position along the tip. We see that the smaller the width is, the smaller is the local longitudinal radius of curvature R_l, and the local residual elastic energy of the configuration. We observed many similar structures in micrographs, but could not evaluate their curvature, because it changes along their length, increasing towards the end. Conversely, observed tips that *could* be fitted satisfactorily with a single circle, we assumed had constant width, i.e., constant protofilament number, along their lengths. We have no rigorous proof that this is so. But it is the simplest possible explanation, and the only plausible one we can think of.

B) Thermal fluctuations included

The microtubule model discussed this far has a *discrete* spectrum of possible radii of curvature, one radius for each protofilament number, as illustrated in Figs. 8 and 10. But this is only because the theory so far has ignored *thermal fluctuations* of tip shapes, i.e., thermal fluctuations that are captured in the samples when they are vitrified for electron microscopy. Thermal forces at room temperature bend entire microtubules, though not by much. Indeed, one measurement of the flexular rigidity of microtubules was based on observations of their thermal fluctuations of shape (Gittes et al. 1993). So significant thermal fluctuations in shape are to be expected for microtubule tips. The mode of lowest energy is the one most significantly excited, and it only changes the radius of curvature of a tip, not its circular shape. If smearing by this lowest mode is wider than the gaps in the discrete spectrum, that spectrum turns into a distribution as smooth as the one in Fig. 2. The observed circular shape of tips then relies on the mode of lowest energy being the only one significantly excited and/or slow enough to be captured by vitrification. Thus, while a discrete spectrum could have confirmed the model, the continuous spectrum we found does not lead to a forthright rejection of it.

So we propose that each line in the sheet model's discrete spectrum for $\tilde{R}_l$ is smeared to the Boltzmann distribution, $\exp(-E(\tilde{R}_l)/k_B T)$, where E is the energy of deformation of tips with a given width and radius $\tilde{R}_l$, k_B is Boltzmann's constant, and T is the absolute temperature. The mode of deformation with lowest energy is a change in radius of curvature, so $\tilde{R}_l$ is the relevant argument for the energy. The energy is approximately quadratic in the curvature $1/\tilde{R}_l$. Then each line in the model's discrete spectrum of radii, $R_n^{(eq)}$, is smeared to a distribution

$$P(R) = A_n \frac{1}{R^2} \exp\left[-B_n\left(\frac{1}{R} - \frac{1}{R_n^{(eq)}}\right)^2\right], \qquad (30)$$

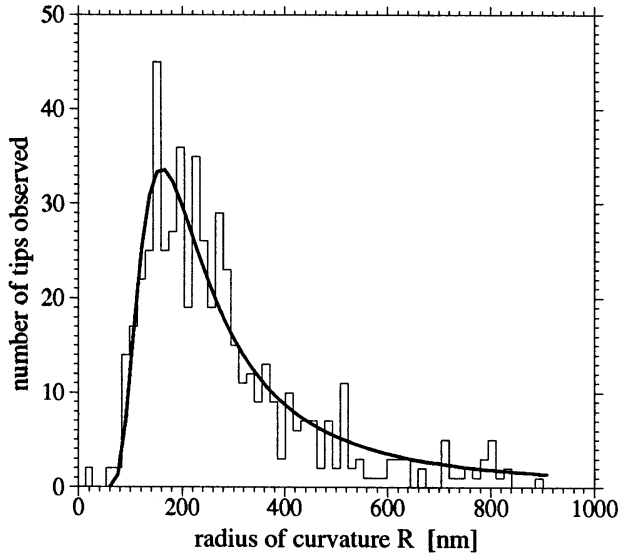

Fig. 12 Fit to the histogram of observed radii from Fig. 2 with single Boltzmann distribution, Eq. (30)

approximately, where A_n is a normalization factor proportional to the number of observed tips made from n protofilaments, and $B_n \propto (K_B T)^{-1}$ characterizes the width of the distribution of observed radii for these tips. This distribution is maximal, equal to A_n, at the radius $R_n^{(eq)}$ that tips made from n filaments have at vanishing temperature.

The fit shown in Fig. 12 is remarkable by how well a single Boltzmann distribution captures the properties of the experimental distribution: its sharp initial rise at low R, its slow decrease at large R, and its overall skewedness, are all perfect. The fact that the distribution in Eq. (30) describes the observed distribution over its range of support from 50 nm to 900 nm, i.e., over a factor 18, strongly indicates that it *is* thermal smearing we see, and shows that the minimum energy mode of deformation can account for what we see.

The bad news is that a good fit by a single Boltzmann distribution indicates that thermal smearing has a width much larger than the gaps in the discrete theoretical spectrum of radii of curvature. If this is correct, the mechanical model for the microtubule can be perfectly correct, but we will be unable to observe the discrete spectrum of radii it predicts, because of the large thermal smear. This because the most obvious and direct test of the model's description of microtubule tips is not possible, unfortunately: while we can observe radii of curvature with precision in electron micrographs, we cannot tell the number of protofilaments in a given tip. If we could, that would provide a decisive test of the scenario we have invoked, since the model predicts a particular correlation between protofilament number and curvature in tips.

V Discussion

The fact that we can set the unknown intrinsic curvature of protofilaments in *growing* microtubule tips equal to the known intrinsic curvature of protofilaments in *shrinking* tips (see Fig. 10), suggests that the difference in tip structure between polymerizing and depolymerizing microtubules needs not necessarily to be caused by active conformational changes of the tubulin. A change in the strength of the lateral bonds between protofilaments, with no significant change within protofilaments, is sufficient to cause the disassembly of a microtubule and the formation of its curly protofilament "crown".

We cannot *prove*, though, that the intrinsic curvature of protofilaments is the same in growing and shrinking microtubules. All we can do is notice that there is no evidence against it. The multi-filament tips observed have shapes consistent with a large built-in curvature in individual protofilaments, we have just shown, and single protofilaments with a small curvature are never observed. Other reasons for the absence of the latter can easily be invented. But what matters here is that they are not observed. Thus we may conclude that identical or similar intrinsic longitudinal curvatures in growing and shrinking microtubules is a possibility.

It would be interesting to repeat the analysis of the present paper for microtubules polymerized from tubulin with non-hydrolyzable GTP analogous. Such an analysis would have one clear advantage over the one presented here: we would know that all tubulin in a tip is liganded with the same analogue, while in the present analysis we cannot exclude the possibility that some is liganded with GTP, and some with GDP. Specifically, it would be known that the single-protofilament extensions, from which we find the intrinsic longitudinal curvature, are made from tubulin having the same ligand as the tubulin in the tips that we model with this intrinsic curvature.

In conclusion, we have reanalyzed experimental data for microtubule tips and found them consistent with a simple elastic sheet model for the microtubule wall. This model explains observed tip geometries in terms of competing intrinsic curvatures in the wall material. The model exhausts existing data, and suggests where further experimental efforts may be aimed.

Acknowledgements We have benefited from discussions with Steve Block, Fred Gittes, Steve Gross, Jonathon Howard, Eric Karsenti, and Stanislas Leibler. I. M. J. acknowledges partial support from the Hungarian National Science Foundation (OTKA) under Grant No. F014967, and thanks the Foundation for Research and Higher Education for a Zoltán Magyary scholarship. H. F. acknowledges partial support form *Julie Damm's Studiefond*.

References

Amost LA, Amos WB (1991) The bending of sliding microtubules imaged by confocal light microscopy. J Cell Sci Suppl 14: 95–101

Bourdieu L, Duke T, Elowitz MB, Winkelmann DA, Leibler S, Libchaber A (1995) Spiral defects in motility assays: a measure of motor protein force. Phys Rev Lett 75:176–179

Chrétien D, Fuller SD, Karsenti E (1995) Structure of growing microtubule ends: two dimensional sheets close into tubes at variable rates. J Cell Biol 129:1311–1328

Chrétien D, Metoz F, Verde F, Karsenti E (1992) Lattice defects in microtubules: protofilament numbers vary within individual microtubules. J Cell Biol 117:1031–1040

Chrétien D, Wade RH (1991) New data on the microtubule surface lattice. Biol Cell 71:161–174

Dye RB, Fink SP, Williams RC Jr (1993) Taxol induced flexibility of microtubules and its reversal by map-2 and tau. J Biol Chem 268:6847–6849

Elbaum M, Fygenson DK, Libchaber A (1996) Buckling microtubules in vesicles. Phys Rev Lett 76:4078–4081

Gittes F, Mickey G, Nettleton J, Howard J (1993) Flexural rigidity of microtubules and actin filaments measured from thermal fluctuations in shape. J Cell Biol 120:923–934

Helfrich W (1973) Elastic properties of lipid bilayers: theory and possible experiments. Z Naturforsch 28c:693–703

Karecla P, Hirst E, Bayley P (1989) Polymorphism of tubulin assembly in vitro. J Cell Sci 94:479–488

Kurachi M, Hoshi M, Tashiro H (1995) Buckling of a single microtubule by optical trapping forces: direct measurement of microtubule rigidity. Cell Motil Cytoskeleton 30:221–228

Kurz JC, Williams RC (1995) Microtubule-associated proteins and the flexibility of microtubules. Biochemistry 34:13347–13380

Landau LD, Lifshitz EM (1959) Theory of elasticity. Pergamon Press, New York

Maaloum M, Chrétien D, Karsenti E, Horber JKH (1994) Approaching microtubule structure with the scanning tunneling microscope. J Cell Science 107:3127–3131

Mickey B, Howard J (1995) The rigidity of microtubules is increased by stabilizing agents. J Cell Biol 130:909–917

Press WH, Teukolsky SA, Vetterling WT, Flannery BP (1992) Numerical Recipes in C, 2nd edn Cambridge University Press, Cambridge

Ray S, Meyerhofer E, Milligan RA, Howard J (1993) Kinesin follows the microtubule protofilament axis. J Cell Biol 121: 1083–1093

Seung HS, Nelson R (1988) Defects in flexible membranes with crystalline order. Phys Rev A 38:1005–1018

Tran PT, Parsons SF, Sterba R, Wang Z, Sheetz MP, Salmon ED (1995) Direct measurement of microtubule flexular rigidity with the laser trap. Mol Biol Cell 6:1509–1509

Vale RD, Coppin CM, Malik F, Kull FJ, Milligan RA (1994) Tubulin GTP hydrolysis influences the structure, mechanical properties, and kinesin-driven transport of microtubules. J Biol Chem 269:23769–23775

Vernier P, Maggs AC, Carlier MF, Pantaloni D (1994) Analysis of microtubule rigidity using hydrodynamic flow and thermal fluctuations. J Biol Chem 269:13353–13360

Voter WA, Erickson HP (1984) The kinetics of microtubule assembly: evidence for a two-stage nucleation mechanism. J Biol Chem 259:10430–10438